ARTICLE IN PRESS

YNIMG-06997; No. of pages: 11; 4C:

NeuroImage xxx (2010) xxx–xxx

Contents lists available at ScienceDirect

NeuroImage

journal homepage: www.elsevier.com/locate/ynimg

The pairwise phase consistency: A bias-free measure of rhythmic neuronal synchronization

Martin Vinck [a,*,1], Marijn van Wingerden [a,2], Thilo Womelsdorf [b,c], Pascal Fries [b,d], Cyriel M.A. Pennartz [a]

[a] Cognitive and Systems Neuroscience Group, Center for Neuroscience, University of Amsterdam, Amsterdam, the Netherlands
[b] Donders Institute for Brain, Cognition and Behaviour, Radboud University Nijmegen, Nijmegen, the Netherlands
[c] Department of Physiology and Pharmacology, University of Western Ontario, Ontario, Canada
[d] Ernst Strüngmann Institute in Cooperation with Max Planck Society, Frankfurt, Germany

ARTICLE INFO

Article history:
Received 23 November 2009
Revised 7 January 2010
Accepted 21 January 2010
Available online xxxx

Keywords:
Rhythmic
Synchronization
Oscillation
Phase-locking
Coherence
Pairwise phase consistency

ABSTRACT

Oscillatory activity is a widespread phenomenon in nervous systems and has been implicated in numerous functions. Signals that are generated by two separate neuronal sources often demonstrate a consistent phase-relationship in a particular frequency-band, i.e., they demonstrate rhythmic neuronal synchronization. This consistency is conventionally measured by the PLV (phase-locking value) or the spectral coherence measure. Both statistical measures suffer from significant bias, in that their sample estimates overestimate the population statistics for finite sample sizes. This is a significant problem in the neurosciences where statistical comparisons are often made between conditions with a different number of trials or between neurons with a different number of spikes. We introduce a new circular statistic, the PPC (pairwise phase consistency). We demonstrate that the sample estimate of the PPC is a bias-free and consistent estimator of its corresponding population parameter. We show, both analytically and by means of numerical simulations, that the population statistic of the PPC is equivalent to the population statistic of the squared PLV. The variance and mean squared error of the PPC and PLV are compared. Finally, we demonstrate the practical relevance of the method in actual neuronal data recorded from the orbitofrontal cortex of rats that engage in a two-odour discrimination task. We find a strong increase in rhythmic synchronization of spikes relative to the local field potential (as measured by the PPC) for a wide range of low frequencies (including the theta-band) during the anticipation of sucrose delivery in comparison to the anticipation of quinine delivery.
© 2010 Elsevier Inc. All rights reserved.

Introduction

Oscillatory activity is abundant in nervous systems and has been implicated in numerous functions (Buzsa'ki and Draguhn, 2004; Fries, 2009; Gray et al., 1989; Pesaran et al., 2002). Two complementary approaches exist for studying oscillations. First, the rhythmic structure of the signals generated by a single source can be examined, for example, by computing the spectral power of EEG (electroencephalogram) or spike signals. Second, one can study the relationship between signals generated by two separate sources, for example, by computing the coherence between neuronal spike output and the LFP (local field potential) or between two EEG or MEG (magnetoencephalography) channels. When the signals generated by two separate sources demonstrate a consistent phase-relationship in a particular frequency-band, then we refer to this property as rhythmic synchronization. Studies have demonstrated task-modulated rhythmic synchronization between local and distant neuronal groups in many different areas and consistent task-modulated phase-relationships of spiking output to the surrounding LFP (Buschman and Miller, 2009; Fries et al., 2008; Fries, 2009; Gregoriou et al., 2009; Lansink et al., 2008; Pesaran et al., 2008; Siapas et al., 2005; Sirota et al., 2008; Womelsdorf et al., 2007).

The two aspects of rhythmic synchronization that are linked to particular functions are the phase of rhythmic synchronization (Fries et al., 2007; Hopfield, 1995; O'Keefe and Recce, 1993; Vinck et al., 2009) and the strength or precision of rhythmic synchronization (Fries, 2005; Sejnowski and Paulsen, 2006; Singer and Gray, 1995; Varela et al., 2001). The consistency of the phase-relationship is typically quantified on the basis of a vector addition operation, i.e., the computation of the resultant vector length (Fisher, 1993), where the vector represents the relative phase between two signals. Two well-known instances of resultant vector length measures in the experimental neurosciences are the PLV (phase-locking value) (Lachaux et al., 1999) and the coherence measure (Mitra and Pesaran, 1999). Unfortunately, measures such as the PLV and the coherence measure have positively biased estimators for finite sample sizes. This

* Corresponding author.
E-mail address: M.A.Vinck@uva.nl (M. Vinck).
[1] MV conceived the original idea of the pairwise phase consistency and was primarily responsible for theoretical and data analysis.
[2] MvW performed the experiments and collected the data.

1053-8119/$ – see front matter © 2010 Elsevier Inc. All rights reserved.
doi:10.1016/j.neuroimage.2010.01.073

Please cite this article as: Vinck, M., et al., The pairwise phase consistency: A bias-free measure of rhythmic neuronal synchronization, NeuroImage (2010), doi:10.1016/j.neuroimage.2010.01.073

is often a particular problem to the neurosciences, wherein data are scarce and the number of observations (trials or spikes) is typically not under the control of the experimenter but varies across subjects or neurons.

Since the bias arises because of the vector addition operation, we might avoid the bias by defining a different kind of measure that avoids this operation completely. In this paper, we propose a new measure of the consistency of phase-relationships, namely, the pairwise phase consistency (PPC). The PPC computes the cosine of the absolute angular distance (the vector dot product) for all given pairs of relative phases, i.e., it computes how similar the relative phase observed in one trial is to the relative phase observed in another trial. We demonstrate that the PPC does not suffer from any bias, because it is based on sequential pairs of observations. Importantly, we prove that the population statistic of the PPC is equivalent to the population statistic of the squared PLV. We compare variance and mean squared error of the PPC and PLV and demonstrate the practical usefulness of the PPC for analyzing actual neuronal data.

Material and methods

The problem of bias in measuring rhythmic synchronization

We are interested in the problem of how to measure whether the signals that are generated by two separate sources demonstrate a consistent phase-relationship in a particular frequency-band. In other words, we want to measure the strength of rhythmic synchronization. In short, this problem will be referred to as how to measure phase consistency. Two of the most widely used measures of phase consistency are the PLV (phase-locking value) and the coherence measure. The PLV and coherence measure have traditionally been quantified for EEGEEG, MEG-MEG or LFP-LFP channel pairs but have also seen successful application on spike–LFP pairs and spike–spike pairs (Jarvis and Mitra, 2001). Central to the definition of the PLV and the coherence measure is the mathematical representation of a complex random variable

$$X_j = r_j exp(i\theta j), \tag{1}$$

where $j = (1, 2, \ldots, N)$, N is the number of observations, $i = \sqrt{-1}$, θ_j is the random relative phase between two signals at a particular frequency-band and r_j is the random non-negative magnitude (usually the product of the channels' magnitudes) that is associated with the relative phase. When the signals are both EEG, MEG or LFP channels, j typically is an index for trial or segment number. When one of the signals is a spike channel and the other signal is an LFP channel, j will typically be an index for spike number. The starting point of our paper is when the relative phases have been determined from the data: We do not consider the important problem of how to optimally determine phases, nor is our technique (pairwise phase consistency, see below) exclusively bound to the use of a particular family of transforms (e.g. wavelet or Fourier). Different approaches exist for determining relative phases: For example, Fourier analysis is often used to obtain a single-phase value per trial, in combination with a particular choice of tapering, such as multitapering (Mitra and Pesaran, 1999), whereas Hilbert or wavelet transform is often used to determine the instantaneous phase as a function of time (Lachaux et al., 1999; Quyen et al., 2001).

We follow the common definition of the sample estimate of the PLV, which we will denote by the symbol Ψ, as

$$\hat{\Psi} \equiv \left| \frac{1}{N} \sum_{j=1}^{N} exp(i\theta j) \right|. \tag{2}$$

Here, the superscript ˆ in $\hat{\Psi}$ indicates that the variable is a sample estimate. We have the bound $0 \leq \hat{\Psi} \leq 1$. The magnitude r_j associated with the relative phase is ignored in the computation of the PLV by normalizing the complex variable X_j to unity before addition. In the context of circular statistics, the PLV corresponds to the resultant length, but here we refer to it in the context of studying rhythmic synchronization between two neuronal sources. The PLV (or resultant length) is an important statistic because it computes the mean of the cosine (real) and sine (imaginary) components of the relative phases and thus indicates whether the data has a circular mean direction. If the resultant length is zero, then both the cosine and sine components of the vectors cancel each other out across observations.

For the coherence, which we denote by the symbol C, we do take amplitude into account. We define $r_j \equiv m_{j1} m_{j2}$, wherein m_{j1} and m_{j2} are the respective channels' non-negative magnitudes.

The standard definition of the sample coherence is

$$\hat{C} \equiv \left| \frac{\sum_{j=1}^{N} mj1mj2\left(i\theta_j\right)}{\sqrt{\left(\sum_{j=1}^{N} m_{j1}^2\right)\left(\sum_{j=1}^{N} m_{j2}^2\right)}} \right| \tag{3}$$

The sample PLV (Eq. 2) and sample coherence (Eq. 3) are estimates of population parameters based on a finite set of observations. The population PLV is defined by the Riemann–Stieltjes integral:

$$\Psi \equiv \left| \int_{-\pi}^{\pi} exp(i\theta)\, dP_\theta(\theta) \right|. \tag{4}$$

Here, the magnitude associated with the relative phase is ignored per definition and $P_\theta(\theta)$ is defined as the cumulative probability distribution function of θ. If the probability distribution of θ is absolutely continuous, then $dP_\theta(\theta) = p(\theta)d\theta$, wherein $p(\theta)$ is a probability density function, and Eq. 4 reduces to $\Psi \equiv | \int_{-\pi}^{\pi} p(\theta) exp(i\theta) d\theta |$. If the probability distribution is discrete, Eq. 4 boils down to $\Psi \equiv | \sum_{k=1}^{K} P_k(\theta = \theta_k) exp(i\theta_k) |$, wherein k is an index for the K discrete probabilities, and $P_k(\theta = \theta_k)$ is the discrete probability of observing the angle θ_k. We write Eq. 4 as a Riemann–Stieltjes integral, because this generalizes the expected values to cases wherein the cumulative probability distribution function is discrete or (absolutely) continuous (the same reason applies to the Riemann–Stieltjes integrals that follow).

The population coherence is defined by the Riemann–Stieltjes integral

$$C \equiv \frac{| \int_0^\infty \int_0^\infty \int_{-\pi}^{\pi} m_1 m_2 exp(i\theta)\, dP(\theta, m_1 m_2) |}{\sqrt{\mathrm{E}\{m_1^2\}\mathrm{E}\{m_2^2\}}} \tag{5}$$

wherein $P(\theta, m_1, m_2)$ is the cumulative joint probability distribution of θ, m_1 and m_2, and the operator E denotes expected value.

Both the estimate of the PLV (Eq. 2) and the coherence (Eq. 3) have bias and variance that are known to depend on the number of observations, such that $\mathrm{E}\{\hat{\Psi}\} \geq \Psi$ and $\mathrm{E}\{\hat{C}\} \geq C$. Both are consistent estimators though, in that $\lim_{N\to\infty} \hat{\Psi} = \Psi$ and $\lim_{N\to\infty} \hat{C} = C$. If we draw a sample of N observations from a population, then the expected value of the PLV estimate (Eq. 2) will decrease as N increases, while the variance across the $\hat{\Psi}$ estimates will decrease. The bias of the PLV is shown in Fig. 2A, wherein we display the average PLV computed for samples generated from a von Mises distribution (Best and Fisher, 1979; Fisher, 1993) with different values of the circular dispersion k and a different number of observations. It is often said that the PLV ranges between 0 and 1. While this is indeed true for a given sample estimate, the expected value of the sample PLV does not range from 0 to 1 but has a dynamic range, which is determined by the sample size and will in practice never approach 0: A completely uniform distribution has a much higher expected value than 0 for small sample sizes.

Please cite this article as: Vinck, M., et al., The pairwise phase consistency: A bias-free measure of rhythmic neuronal synchronization, NeuroImage (2010), doi:10.1016/j.neuroimage.2010.01.073

The finite sample size bias can be informally explained by the following example. Suppose that our relative phases are drawn from the uniform circular distribution, which has probability density $p(\theta) = \frac{1}{2\pi}$. In other words, every phase is equally likely to be observed. If the sample size N goes to infinity, we would expect that all phases cancel each other out, such that the PLV approaches zero, i.e., $\Psi = |\int_{-\pi}^{\pi} \frac{1}{2\pi} exp(i\theta) d\theta| = 0$. However, the expected circular distance between any pair of relative phases θ_j and θ_k (where j and k are indices for different trials or spikes) is equal to $\frac{1}{2}\pi$ (90°). Thus, if we have only two observations, our resultant length is expected to be larger than zero. Precisely, for two observations x and y, the expected value of our sample PLV will be equal to

$$\mathrm{E}\left\{\hat{\Psi}\right\} = \int_{-\pi}^{\pi} \frac{1}{4\pi} \sqrt{((1 + \cos x)^2 + (\sin x)^2)} dx = \frac{2}{\pi}. \tag{6}$$

Here, we rotated both phases such that $y = 0$ and only the variable x remains, and $\cos(y) = 1$ and $\sin(y) = 0$. If we now add a third observation, then the average distance of the new observation to the resultant vector of the first two observations will again be $\frac{1}{2}\pi$, which will lead to a smaller resultant length. This process goes on until the resultant length reaches the value of zero (because the distribution is uniform).

The finite size sample problem is complicated by the fact that the way $\hat{\Psi}$ decreases as a function of the sample size depends on the type of circular distribution. Suppose we have as a probability distribution $P(\frac{1}{2}\pi) = \frac{1}{2}$ and $P(-\frac{1}{2\pi}) = \frac{1}{2}$. As with the uniform circular distribution, the population PLV (Eq. 4) is zero for this distribution. Suppose that the sample consists of two observations. Either the observed phases are equal to each other, thus the circular distance will be zero, or they are orthogonal to each other, thus they cancel each other out completely. Thus, the expected resultant length for two observations will be $E\left\{\hat{\Psi}\right\} = \frac{1}{2} \cdot 1 + \frac{1}{2} \cdot 0 = \frac{1}{2}$. Suppose that the sample consists of three observations. Then, we have $(2)^3 = 8$ possible outcomes, wherein two of the eight cases all observed phases are identical, such that $\hat{\Psi} = 1$ for those observations. For all other possible outcomes, we have two identical phases and one orthogonal phase, such that $\hat{\Psi} = \frac{1}{3}$. We thus have $E\{\hat{\Psi}\} = \frac{1}{4} \cdot 1 + \frac{3}{4} \cdot \frac{1}{3} = \frac{1}{2}$. Thus, $\hat{\Psi}$ converges in a non-continuous way to the population PLV (Eq. 4). Fig. 2B compares the dependence of $\hat{\Psi}$ on the sample size for this distribution with the uniform distribution. Both distributions have the same population PLV (Eq. 4), but the expected value of the sample estimate of the PLV (Eq. 2) converges in a very different way to the population PLV. Any correction to $\hat{\Psi}$ thus depends on the assumption of a particular circular distribution.

Reducing the bias by fixing the number of spikes

Recently (Vinck et al., 2009; Womelsdorf et al., 2008), we introduced a technique to reduce the positive bias of the sample PLV and sample coherence estimate (Eqs. 2 and 3). We suggested that we can reduce this bias by using the same number of observations for every sample when comparing samples with a different number of observations. For example, if we have a thousand trials in the first sample and 50 trials in the second, we can reduce the bias by using only 50 observations from the first sample to compute the PLV. To use all available data, a bootstrap without replacement (i.e., every observation can enter one bootstrapped sample only once) can be used to reduce the variance of the new estimates. Thus, we introduced the FSPLV (fixed-sample size PLV) estimate as

$$\hat{\Psi}^f \equiv \frac{1}{BF} \sum_{b=1}^{B} \left| \sum_{j=1}^{F} exp\left(i\theta_{jb}\right) \right|, \tag{7}$$

where $b = (1, 2, \ldots, B)$, with B as the number of bootstrapswithout replacement and F as the fixed number of spikes, with $F \leq N$.

We argue that the FSPLV (see also the discussion for a direct comparison with the pairwise phase consistency) still copes with several disadvantages: First, because the bias curves depend on the type of circular distribution, as shown in Fig. 2B, we can only compare the FSPLV between two samples in an unbiased way when they are drawn from the same probability distribution (that can have different parameters). Bimodal or even more complex phase distributions are not uncommon in neuronal data. For example, very strong phase-locking at a higher frequency can cause a bimodal phase distribution at the lower harmonic. Thus, when samples drawn from two different types of distributions are compared, a systematic difference between their samples' FSPLV may arise, even though the population FSPLV can be the same for the two distributions. Second, one has to choose the arbitrary parameter F, and different choices of this parameter might lead to systematically different conclusions. Moreover, if different parameter values of F are chosen across different experiments, it will be hard to compare the degree of phase consistency across experiments, because we are essentially using a different population statistic in every experiment. Third, it is not practical to use all available data in the same way, because computing all possible bootstraps is computationally not feasible. For example, if we have 10,000 observations, the number of unique bootstraps of size 50 equals $\binom{10000}{50}$. That means that some observations might be used more often than other observations and that some combinations of observations are not taken into account. This will lead to a higher variance of our sample estimates and also a variance of the outcomes from run to run.

The pairwise phase consistency

The main problem with the sample estimate of the resultant length (or PLV) is that its finite sample estimator is biased by the number of observations. A measure that does not depend on the number of observations is suggested by looking at pairs of observations instead of all observations together. If phases are consistently clustering around some mean phase, they will on average have a small angular distance to each other.

We first introduce the average pairwise circular distance (APCD), which computes the absolute angular distance between relative phases. The APCD is defined by

$$\hat{D} \equiv \frac{2}{N(N-1)} \sum_{j=1}^{N-1} \sum_{k=(j+1)}^{N} d\left(\theta_j, \theta_k\right), \tag{8}$$

wherein $d(\varphi,\omega)$ is the absolute angular distance defined as the function

$$d(\varphi, \omega) \equiv |\varphi - \omega| \bmod \pi \tag{9}$$

and θ_j and θ_k are the relative phases from two observations (j and k are indexing trials or spikes). There are in total $\binom{N}{2}$ unique pairs that are composed of different observations. In essence, D computes the average absolute angular distance between all observed relative phases.

We define the population APCD by the Riemann–Stieltjes integral

$$D \equiv \int_{-\pi}^{\pi} \int_{-\pi}^{\pi} d(\varphi, \omega) dP_{\varphi}(\varphi) dP_{\omega}(\omega). \tag{10}$$

Here, $P_{\varphi}(\varphi) = P_{\omega}(\omega)$ is defined as the cumulative probability distribution of the relative phase θ_j. If the random variables φ and ω are absolutely continuously distributed, then $dP_{\varphi}(\varphi) dP_{\omega}(\omega) = p(\varphi) p(\omega) d_{\varphi} d\omega$, and Eq. 10 reduces to the standard (Riemann) integral $D \equiv \int_{-\pi}^{\pi} \int_{-\pi}^{\pi} p(\varphi) p(\omega) d(\varphi, \omega) d\varphi d\omega$.

To obtain a measure which has a similar dynamic range as the PLV and the coherence, we normalize the APCD, giving rise to a new

Please cite this article as: Vinck, M., et al., The pairwise phase consistency: A bias-free measure of rhythmic neuronal synchronization, NeuroImage (2010), doi:10.1016/j.neuroimage.2010.01.073

measure, which we call the pairwise circular distance index (PCDI) and which we will denote by the symbol $D^{\star}$.

The PCDI is defined as

$$\hat{D}^{\star} = \frac{\pi - 2\hat{D}}{\pi} \tag{11}$$

where the superscript $\star$ in $D^{\star}$ indicates normalization. We have $-1 \leq D^{\star} \leq 1$, and $0 \leq D^{\star} \leq 1$, with a value of 1 indicating complete phase consistency (corresponding to an average distance between pairs of 0) and a value of 0 indicating a complete absence of phase consistency, which is the case for example with the uniform circular distribution or a mixture of two von Mises distributions with an orthogonal mean phase and equal dispersion.

An important question pertains to what the relationship is between the population value of the PLV (or resultant length) and the APCD and PCDI. Obviously, the resultant vector length is a very important circular statistic, because it indicates whether the data have an angular mean direction. The angular distance (Eq. 9) can be alternatively written as $d(\varphi, \boldsymbol{\omega}) = \arccos\,(\cos(\varphi)\cos(\boldsymbol{\omega}) + \sin(\varphi)\sin(\boldsymbol{\omega}))$. This leads to the following relationship between the PLV and the APCD: We can rewrite the PLV as

$$\Psi \equiv \sqrt{\left(\int_{-\pi}^{\pi} \cos(\theta) dP_{\theta}(\theta)\right)^2 + \left(\int_{-\pi}^{\pi} \sin(\theta) dP_{\theta}(\theta)\right)^2}. \tag{12}$$

Hence we have the squared PLV as

$$\begin{aligned} \Psi^2 &\equiv \left(\int_{-\pi}^{\pi} \cos(\theta) dP_{\theta}(\theta)\right)^2 + \left(\int_{-\pi}^{\pi} \sin(\theta) dP_{\theta}(\theta)\right)^2 \\ &= \int_{-\pi}^{\pi}\int_{-\pi}^{\pi} (\cos(\theta)\cos(\boldsymbol{\omega}) + \sin(\theta)\sin(\boldsymbol{\omega})) dP_{\theta}(\theta) dP_{\boldsymbol{\omega}}(\boldsymbol{\omega}). \end{aligned} \tag{13}$$

The population statistic of the APCD (Eq. 16) is equivalent to the population statistic of the squared PLV, expect for an arccosine transformation of the dot product inside the integral. The relationship between the APCD and the PLV implies that we can define a pairwise statistical measure, which gives an unbiased estimate of the population statistic of the squared PLV. We call this measure the pairwise phase consistency (PPC) and denote it by the symbol Υ. We have the sample estimate of the PPC as

$$\hat{\Upsilon} \equiv \frac{2}{N(N-1)} \sum_{j=1}^{N-1} \sum_{k=(j+1)}^{N} f\left(\theta_j, \theta_k\right), \tag{14}$$

wherein the function f computes the dot product between two unit vectors and is defined by

$$f(\varphi, \boldsymbol{\omega}) \equiv \cos(\varphi)\cos(\boldsymbol{\omega}) + \sin(\varphi)\sin(\boldsymbol{\omega}). \tag{15}$$

The population statistic of the PPC is given by $\Upsilon = \Psi^2$ (Eq. 13).

The sample estimate is bound by $-1 \leq \hat{\Upsilon} \leq 1$. The PPC has an essential advantage in comparison to the PCDI: The expected value of its estimator is equal to the population statistic of the squared value of the resultant length (PLV). The relationship between the APCD and the PPC is given by taking the cosine of the absolute angular distances,

$$\Upsilon \equiv \int_{-\pi}^{\pi}\int_{-\pi}^{\pi} \cos(d(\varphi, \boldsymbol{\omega})) dP_{\varphi}(\varphi) dP_{\boldsymbol{\omega}}(\boldsymbol{\omega}). \tag{16}$$

The PPC is graphically explained in Fig. 1.

The key difference between the APCD and the PPC is that for the computation of the APCD, we determine the absolute angular distances between relative phases, whereas for the computation of the PPC, we determine the cosine of the absolute angular distances. For angular differences close to 90° ($\frac{1}{2\pi}$), the angular distance and the cosine of the angular distance are approximately linearly related, since for these angles we have $\cos(x) \approx \frac{1}{2}\pi - x$. However, especially

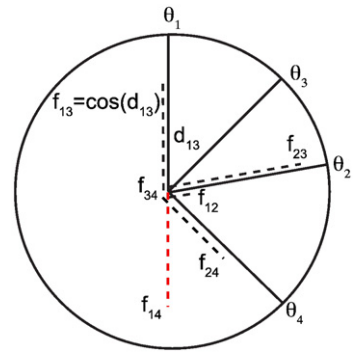

Fig. 1. Explanation of the PPC. Each solid line represents an observation of the relative phase between two different signals at a particular frequency. Pairs are composed of all different observations. In total there are 1/2*N*(*N* Explanation of the PPC. Each solid line represents an observation of the relative phase between two different signals at a particular frequency. Pairs are composed of all different observations. In total there are 1/2*N*(*N* − 1) unique pairs. In this case there are four observations, hence six unique pairs. For every pair, the angular distance between two vectors can be computed. For example, the angular distance between θ_1 and θ_3 is indicated by d_{13} and is equal to 45°. If phase consistency is high, then the relative phases will have small angular distances relative to each other. For every pair, we now compute the dot product between the two vectors, which equals to cosine of the angular distance, i.e., the projection of one vectors onto another vector. These are indicated with dotted lines. Red lines indicate a negative dot product, i.e., an angular distance greater than 90 , and black lines a positive dot product. The PPC is equal to the average dot product across all pairs and provides an unbiased estimate of the squared PLV. Note that the angle between θ_4 and θ_3 equals 90 , hence the dot product is zero. The average dot product is greater than zero, indicating that there is a circular mean direction. PPC is lower than squared PLV. (For interpretation of the references to colour in this figure legend, the reader is referred to the web version of this article.)

for small distances and for very large angular distances, the functions $d(\varphi, \theta)$ (Eq. 9) and $f(\varphi, \theta)$ (Eq. 15) behave differently, since the derivative of the cosine of the angular distances is zero for these angular distances.

There exist distributions for which the PLV is zero, but the PCDI is not. In other words, for these distributions there is no circular mean direction, but the mean angular distance between relative phases is smaller than 90°. For example, suppose we have a circular distribution with probabilities defined by $P(\theta = \frac{1}{2}\pi) = \frac{\sqrt{2}}{2+\sqrt{2}}$, $P(\theta = 1\frac{1}{4}\pi) = \frac{1}{2+\sqrt{2}}$ and $P(\theta = \frac{1}{4}\pi) = \frac{1}{2+\sqrt{2}}$ for this distribution is zero, but the PCDI is not. The APCD is given by

$$\begin{aligned} D &= \frac{1 \cdot 1 \cdot 2}{\left(2+\sqrt{2}\right)^2} \cdot \frac{1}{2}\pi + \frac{\sqrt{2} \cdot 1 \cdot 2 \cdot 2}{\left(2+\sqrt{2}\right)^2} \cdot \frac{3}{4}\pi \\ &= \frac{2+6\sqrt{2}}{2+\left(4+2\sqrt{2}\right)\sqrt{2}} \cdot \frac{1}{2}\pi \leq \frac{1}{2}\pi \end{aligned} \tag{17}$$

On the contrary, the PPC is given by

$$\Upsilon = \frac{2 \cdot 2 \cdot 1 \cdot \sqrt{2} \cdot \left(-\frac{1}{2}\sqrt{2}\right)}{\left(2+\sqrt{2}\right)^2} + \frac{\sqrt{2} \cdot \sqrt{2} + 1 \cdot 1 + 1 \cdot 1}{\left(2+\sqrt{2}\right)^2} = 0 \tag{18}$$

Bias and variance of the sample PPC estimator

In this paragraph, we will show that the sample estimator of the PPC is consistent and not biased by the sample size. The expected value of the sample PPC equals

$$\begin{aligned} \mathrm{E}\left\{\hat{\Upsilon}\right\} &= \mathrm{E}\left\{\frac{2}{N(N-1)} \sum_{j=1}^{N-1} \sum_{k=(j+1)}^{N} d\left(\theta_j, \theta_k\right)\right\} \\ &= \frac{2}{N(N-1)} \sum_{j=1}^{N-1} \sum_{k=(j+1)}^{N} \mathrm{E}\left\{d\left(\theta_j, \theta_k\right)\right\} \\ &= \Upsilon. \end{aligned} \tag{19}$$

Here, we used the property $E\{f(X1, X2) + f(X2, X3)\} = E\{f(X1, X2)\} + E\{f(X2, X3)\}$ and the assumption that $dP(\theta_j, \theta_k) = dP(\theta_j)\, dP(\theta_k)$, in other words that our observations are independent. Eq. 19 shows that the expected value of the sample PPC does not depend on the number of pairs in our sample. The pairs are of course not independent, but this does not affect the expected value, but the variance of our sample estimate. The variance of our sample PPC estimate is given by

$$\mathrm{Var}\left\{\hat{\Upsilon}\right\} = \mathrm{E}\left\{\hat{\Upsilon}^2\right\} - \Upsilon^2 \tag{20}$$

We have

$$\mathrm{E}\left\{\hat{\Upsilon}^2\right\} = \mathrm{E}\left\{\frac{4}{N^2(N-1)^2}\left(\sum_{j=1}^{N-1}\sum_{k=(j+1)}^{N} d\left(\theta_j, \theta_k\right)\right)^2\right\}. \tag{21}$$

We can decompose $\mathrm{E}\{\hat{\Upsilon}^2\}$ in three terms: The product of the distance for pairs that are identical, the product of the distance for pairs that are independent and the product for pairs in which there is one shared observation, such that the total number M of product of pairs (for $N>3$) equals

$$\begin{aligned} M &= \binom{N}{2} + \binom{N}{2}\frac{(N-2)(N-3)}{2} + \binom{N}{2}(2N-4) \\ &= \binom{N}{2}^2. \end{aligned} \tag{22}$$

The variance of the PPC estimate is thus given by

$$\begin{aligned} \mathrm{Var}\left\{\hat{\Upsilon}\right\} = {} & \frac{2}{N(N-1)}\int_{-\pi}^{\pi}\int_{-\pi}^{\pi} f(\omega,\vartheta)^2 dP_{\vartheta}(\vartheta) dP_{\omega}(\omega) \\ & + \frac{6-4N}{N(N-1)}\Upsilon^2 \\ & + \frac{4N-8}{N(N-1)}\int\int\int_{-\pi}^{\pi} f(\varphi,\vartheta)^2 f(\varphi,\omega) dP(\varphi) dP(\vartheta) dP(\omega) \end{aligned} \tag{23}$$

and the function f is defined by Eq. 9. This means that the variance of the PPC estimate approaches zero asymptotically,

$$\lim_{N\to\infty} \mathrm{Var}\left\{\hat{\Upsilon}\right\} = 0. \tag{24}$$

The asymptote of our estimate $\hat{\Upsilon}$ is thus equal to

$$\lim_{N\to\infty} \hat{\Upsilon} = \Upsilon. \tag{25}$$

This demonstrates that $\hat{\Upsilon}$ is a consistent and unbiased estimator of Υ. Note that Eqs. 19–25 applies to the PCDI as well.

Simulations based on artificial data

To compare the variance and mean squared error between the squared PLV and the PPC and to validate our analytical findings by means of numerical simulations, we created artificial samples drawn from a von Mises distribution, according to (Best and Fisher, 1979). For every sample drawn, we computed the PLV, the squared PLV, the PCDI and the PPC. We repeated this procedure 10^6 times to obtain estimates of the variance and the mean of the PLV, the squared PLV, the PCDI and the PPC. We repeated this procedure for a large range of the dispersion parameter K from the von Mises distribution. The population PLV and squared PLV values are respectively given by

$$\Psi = \frac{I_1(K)}{I_0(K)}, \tag{26}$$

and Ψ^2, wherein $I_1(K)$ and $I_0(K)$ are modified Bessel functions of order zero and one, and K is the dispersion parameter from the von Mises distribution (Fisher, 1993). The MSE of the sample estimates is defined as

$$MSE \equiv \frac{1}{M}\sum_{m=1}^{M}\left(\hat{S}_m - S\right)^2, \tag{27}$$

wherein m is the index for sample number, M is the total number of samples that we draw from the population, and $\hat{S}$ is the sample estimate of the population statistic S (either PLV or PPC). All simulations were performed in C using the gcc compiler.

Actual spike–LFP data

Three adult male Wistar rats (Harlan CPB, Horst, the Netherlands), weighing 370–450 g at the time of surgery, served as subjects in these experiments. Prior to training and surgery, the rats were housed two to a cage on a reversed light/dark cycle (lights off: 7AM, lights on: 7PM) with ad libitum food and water. After surgery, animals were housed individually in a transparent cage (40×40×40 cm), with other rats present in the climate controlled colony room. During training and recording, rats were maintained on food restriction, with 5–15 g of food available from $>\frac{1}{2}$ h after training, depending on the amount of reward collected in the session, amounting to 90% free-feeding intake. All experiments were conducted according to the National Guidelines on Animal Experiments and with approval of the Animal Experimentation Committee of the University of Amsterdam.

Odor discrimination training was conducted in an operant chamber (56×30×40 cm L W H). The chamber was equipped with an odor sampling port and trial light on a front panel and a tray for delivery of fluids placed at the opposing wall. The front panel was slanted at 45 (with respect to ground level) above the odor sampling port to allow unhindered nose poking into the odor port by implanted animals. Entries by the animals into the odor port, fluid well and licking into the well were recorded by photobeam interruptions. During recording sessions, behavioral events were synchronized with electrophysiological data acquisition running on a separate computer. Odors were delivered via separate glass vials and tubing to avoid mixing. Upon entering the application system, they were mixed 1:1 with clean air and released into the compartment directly behind the odor port by way of computer-controlled valves. Likewise, quinine and sucrose solutions were delivered to the fluid well via separate fluid lines and electronically controlled by valves. Training and task performance were devoid of human interference. The animals were trained on a two-odor go/no-go discrimination task. After habituation to the chamber and pre-training, rats were confronted with odor discrimination problems. Each session, one novel odor was associated with reward (100 μl of 15% sucrose solution), and a second novel odor with an aversive outcome (100 μl of 0.01 M quinine solution). Training sessions consisted of blocks of 5 + 5 pseudo-randomly ordered positive and negative odor trials. When a trial light was illuminated, rats could initiate a trial by poking their snout in the odor sampling port. After a 500-ms delay, air flow through the odor sampling port was switched from clean air to the selected clean air/odorant mixture. A correct nose poke in the odor port (wait for odor 500 ms, constituting a pre-stimulus delay, and sample odor for at least 750 ms) was indicated by the trial light turning off. After sampling, the rats could move over to the fluid well, into which they were required to make a nose poke for >100 ms before the outcome (sucrose or quinine solution) was presented. We refer to the invariant 1000-ms delay period as the anticipatory period. This anticipation period allows sampling of neural activity during the waiting period that is not confounded by whole-body movement. When the rats left the fluid well, an inter-trial interval (ITI) of 10–15 s was observed before the

next trial started. A correct rejection was scored if the rat refrained from entering the reinforcement tray for >5 s following sampling of the negative odor. Responses during the ITI had no programmed consequences, while prematurely ended responses (i.e., short pokes) during the odor sampling or waiting period resulted in immediate termination of the current trial and the start of a new trial.

Rats were implanted after they reached behavioral criterion, viz. scoring >85% hits and correct rejections over a moving block of 20 trials. Animals were anesthetized by i.m. injection of 0.08 ml/100 g Hypnorm (0.2 mg/ml fentanyl, 10 mg/ml fluanison; VetaPharma Ltd., Leeds, UK), followed by 0.04 ml/100 g. Dormicum (5 mg/ml midazolam; Roche Nederland B.V., Woerden, the Netherlands) s.c. and mounted in a stereotact. Body temperature was maintained between 35 and 36 °C. A microdrive, holding 14 individually moveable electrode drivers, was chronically implanted onto a craniotomy (diameter: 2 mm) in the left hemisphere dorsal to the OFC at 3.4–3.6 mm anterior and 3.0–3.2 mm lateral to bregma. The drivers were loaded with 12 tetrodes and 2 reference electrodes. Using dental cement, the drive was anchored to six stainless steel screws, one of which was positioned in the left parietal bone and served as ground. Immediately after surgery, all tetrodes and reference electrodes were advanced 0.8 mm into the brain. Next, the animal was allowed to recover for 7 days with ad libitum food and water, during which the 12 recording tetrodes were advanced in daily steps to the upper border of the OFC according to a standardized rat brain atlas (Paxinos and Watson, 1982). The reference electrodes were lowered to a depth of 1.2–2.0 mm and adjusted to minimize spiking activity on the reference channel. After surgery, saline was injected s.c. (2 ml per flank), and pain relief was provided by 0.1 ml/100 g pre-surgical weight of a 10% Finadyne (flunixin meglumine 50 mg/ml; Schering-Plough, Brussels, Belgium) solution administered in saline s.c.

Following surgery, animals were retrained on the familiar odor pair with which initial training took place until performance was back at criterion level. Recording of neural activity started in the subsequent session. On each recording session, rats were confronted with a new odor pair. Using tetrodes, neural activity was recorded by a 64-channel Cheetah setup (Neuralynx, Bozeman MT). Signals were passed through a unity-gain pre-amplifier headstage, a 72-channel commutator (Dragonfly, Ridgeley, West Virginia, USA), amplified 5000 and bandpass filtered between 600 and 6000 Hz for spike recordings. If a signal on any of the leads of a tetrode crossed a pre-set threshold, activity on all four leads was sampled at 32 kHz for 1 ms and stored for off-line analysis. Local field potentials recorded on all tetrodes were amplified 1000 , continuously sampled at 1874 Hz, and bandpass filtered between 1 and 475 Hz. Events in the behavioral task were co-registered and time-stamped by the Cheetah system. Spike trains were sorted to isolate single units using a semi-automated clustering algorithm (BubbleClust) followed by manual refinement using MClust. Automated and manual clustering of spikes was done using the waveform peak amplitude, area, squared amplitude integral and the first three principal components. Clusters were accepted as single units when having no more than 0.1% of inter-spike intervals shorter than 2 ms.

All data analysis was performed in MATLAB, with additional use of the Fieldtrip Toolbox and custom-made Mex-files, using the gcc compiler. For every neuron, we computed the spike–LFP phase for every spike by Fast Fourier Transforming an LFP segment of length T samples,

$$X_j(f) = \sum_{t=1}^{T} w(t)x_j(t)exp(i2\pi ft). \tag{28}$$

Here, $w(t)$ is a Hanning window, $x_j(t)$ is the unfiltered LFP segment that is centered around the spike, f is the frequency, and j is an index for spike number.

Results

Simulations based on artificial data

We first tested whether the PPC (pairwise phase consistency) indeed has a bias-free sample estimator by computing the PPC for samples drawn from a von Mises distribution with different sample sizes and levels of dispersion. Fig. 3A shows that the PPC does not have any bias a function of the sample size, as we predicted analytically by Eq. 19. As predicted from Eqs. 13 and 16, we observed identical population values for the PPC and the squared PLV (Fig. 3B). In addition, for samples drawn from a von Mises distribution, we obtained a near linear relationship between the population squared PLV (phase-locking value) and the population PCDI (pairwise circular distance index) for a large range of the population PLV (PLV<0.9) (Fig. 3B). We can approximate the population squared PLV with great accuracy by $\Psi^2 = \beta D^\star$ wherein $\beta = 1.21$ and Ψ and $D^\star$ are defined respectively by Eq. 2 and Eq. 11.

Typically, a reduction in bias for some estimator comes at the expense of an increase in variance and MSE (mean squared error). Thus, we were interested in comparing the MSE and variance of the PPC with the squared PLV. For a given value of the von Mises dispersion parameter K, the population statistics of both statistics are known and derived from Eq. 26. Fig. 3C compares the log ratio of the MSE of the PPC to the MSE of the squared PLV. A value of zero indicates that the MSE is the same for both statistics. Values lower than zero indicate that MSE is smaller for the PPC than for squared PLV. For small values of the population PLV (0–0.3), where the bias and variance problem is most severe, the MSE of the PPC compares favorably to the MSE of the squared PLV. For higher values of the PLV (0.4–1), the MSE of the PPC is only slightly greater than the MSE of squared PLV. Fig. 3D displays the difference in variance of the squared PLV with the variance of the PPC. A value of zero indicates that the variance is equal, whereas a higher value than zero indicates that the variance of the PPC is relatively higher. For small samples (N<10), the PPC estimate suffers from higher variance than the squared PLV estimate, showing that there is some trade-off between bias and variance. It should be noted however, that for small sample sizes (e.g., $N = 2$), the PPC has a dynamic range that still extends from 0 to 1, whereas the squared PLV has a much smaller dynamic range (the lower bound is pushed towards 1 because of the bias). Given a fixed variance, we are less sensitive in detecting differences in the population statistic if the dynamic range of the sample estimate is smaller.

Analysis of neuronal data

We first verified that our technique indeed provides unbiased results for actual neuronal data. For that purpose, we selected cells from which we recorded more than 200 spikes during the period in which the rat anticipated sucrose delivery at the fluid well, in order to obtain a relatively smooth circular distribution of spike theta (6 Hz) phases. The sample of all recorded spikes now functioned as the population probability distribution. Then, for every selected neuron, we drew small-size samples of spike phases from the distribution of all recorded spike phases. Samples were drawn without replacement. Draws were repeated 50,000 times to obtain an estimate of the expected value of the sample estimates. Fig. 4A shows that there was a negative relationship between the expected value of the PLV estimates and the sample size, similar to the results of the numerical simulations shown in Fig. 2A. As predicted (Fig. 3A and Eq. 19), no systematic bias was observed when using the PPC (Fig. 4B). This means that for the expected value of our PPC sample estimate, it would not have made a difference whether we observed 200 or 10 spikes from a given neuron (of course, for the variance it would).

Next, we computed the PLV and PPC for every neuron using all available spikes and compared the PLV (Fig. 4C) and PPC (Fig. 4D)

Please cite this article as: Vinck, M., et al., The pairwise phase consistency: A bias-free measure of rhythmic neuronal synchronization, NeuroImage (2010), doi:10.1016/j.neuroimage.2010.01.073

across the neuronal population. For cells with small sample sizes (few spikes), we observed much higher PLVs and a higher variance. Figs. 4C and D demonstrate an important downside of the FSPLV when applied to spike data, namely: The number of spikes we choose to compute the FS-PLV will lead to a selection of only a subset of neurons that have a higher number of spikes (and likely higher firing rates) than on average, for example, interneurons or neurons that increase their firing rate during the period under consideration. Conclusions drawn from analyses on this subset of neurons might not generalize to the population of all cells, especially since neurons with a large number of spikes might have different firing rate correlates.

As a demonstration, we then examined the relationship between task conditions (rat behavior) and the PPC spectra. We investigated the structure of PPC spectra for different inclusion criteria for our cells (i.e., the minimal number of spikes that was required to include a cell). Figs. 5A–D show the PPC spectra for the sucrose waiting (positive outcome; 1000 ms before fluid delivery) and quinine waiting (negative outcome; 1000 ms before fluid delivery) task periods. During this period, orbitofrontal cortex neurons are selective by means of their firing rate for the upcoming task outcome, based on a cue that was received a few seconds before (one of two odors). Every plot represents a different number of minimal spikes that had to be recorded from a neuron before we included it (2, 10, 30, 50). As Fig. 4D shows, when the minimal number of spikes is small, neurons are included whose individual sample estimates have a high variance (especially when they are weakly locked), which might obscure differences between task conditions. Figs. 5A–D show that theta-band spike–LFP phase-locking is enhanced during the sucrose waiting period relative to other task periods. Even when all cells are included, regardless of their sample size, we obtain similar results, showing that the difference in theta-band rhythmic synchronization between the sucrose and the quinine waiting period holds at the level of the complete sample of recorded cells, not only for the sample of cells with a relative high firing rate. Second, we show that across a large range of frequencies (2 to 10–15 Hz), rhythmic synchronization is selectively enhanced during the sucrose waiting period versus the quinine waiting period.

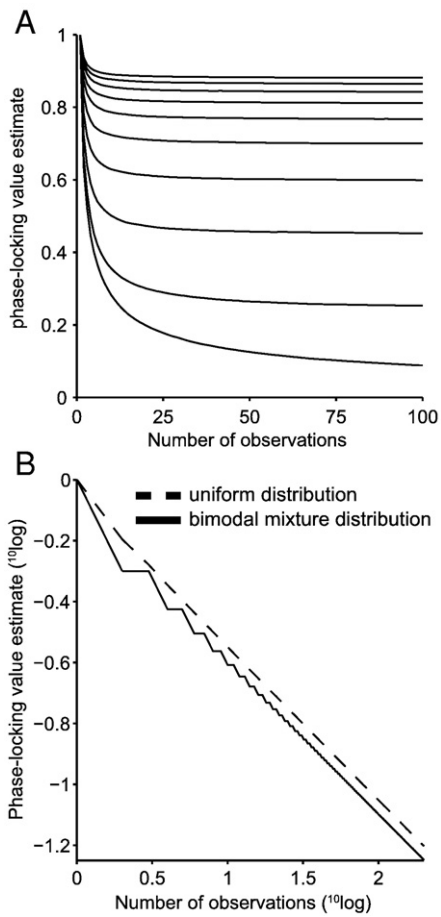

Fig. 2. Bias of phase-locking value (PLV) estimate. (A) PLV estimate versus sample size. PLV estimate is most strongly biased for small PLV values and small sample sizes. Samples were drawn from a von Mises distribution. Different lines correspond to different values of the concentration parameter of the von Mises distribution. Line with lowest PLV corresponds to the uniform distribution. (B) Sample-size bias of PLV estimate depends on circular distribution type. PLV estimate (on logarithmic scale) versus sample size (in logarithmic scale). Dotted line: PLV estimate for uniform distribution. Solid line: PLV estimate for bimodal distribution (mixture of orthogonal dirac delta distributions). Both distributions have a population PLV of 0. However, the PLV estimate for the bimodal distribution is a non-differentiable function of sample size and converges more rapidly to its population parameter. Bias of phase-locking value (PLV) estimate. (A) PLV estimate versus sample size. PLV estimate is most strongly biased for small PLV values and small sample sizes. Samples were drawn from a von Mises distribution. Different lines correspond to different values of the concentration parameter of the von Mises distribution. Line with lowest PLV corresponds to the uniform distribution. (B) Sample-size bias of PLV estimate depends on circular distribution type. PLV estimate (on logarithmic scale) versus sample size (in logarithmic scale). Dotted line: PLV estimate for uniform distribution. Solid line: PLV estimate for bimodal distribution (mixture of orthogonal dirac delta distributions). Both distributions have a population PLV of 0. However, the PLV estimate for the bimodal distribution is a non-differentiable function of sample size and converges more rapidly to its population parameter.

Discussion

We investigated the problem of how to measure phase consistency, i.e., whether signals that are generated by two separate sources display a consistent phase-relationship in a particular frequency-band. The sample estimators of the PLV (phase-locking value) and the coherence measure are strongly biased by the number of observations (trials or spikes) in the sample. This bias is difficult to control, because the way the bias behaves depends on the circular distribution (for example, unimodal versus bimodal). We have introduced the pairwise phase consistency (PPC) as a new measure of phase consistency. We demonstrated analytically, by means of simulations and by application on actual neuronal data, that the sample estimate of the PPC is an unbiased and consistent estimator of the population PPC. These properties, unbiasedness and consistency, hold independently of the circular distribution of the relative phases. We demonstrated, both analytically and by means of simulation, that the population statistic of the PPC is identical to the population statistic of the squared PLV. This means that we can interpret the PPC both in terms of (the cosine of) angular distances and in terms of the population value of the squared PLV. Furthermore, we showed that the MSE (mean square error) of the PPC estimate compared favorably to that of the squared PLV for low values of the PLV (0–0.3), where the problems of variance and bias are most severe. Finally, we demonstrated the use of the PPC in actual neuronal data. Thus, the PPC and the squared PLV have the same population statistic, but the key advantage of the PPC is that it has a bias-free sample estimator. In addition, we introduced the pairwise circular distance index (PCDI), which computes the absolute angular distances between relative phases. Although the PCDI has an unbiased and consistent estimator, it is more difficult to interpret the PCDI than it is to interpret the PPC: Although for a large range of dispersion of relative phases ($R<0.9$), we demonstrated by numerical simulations that there is a linear relationship between the PCDI and the population value of the squared PLV for a von Mises distribution, the relationship between the PCDI and the population value of the (squared) PLV remains to be investigated for other probability distributions, for example, probability distributions that are not unimodal. For a uniform distribution, the PCDI and PLV are both zero, but we have shown that for example for a trimodal probability distribution, the PLV can be zero, while the PCDI is not.

Please cite this article as: Vinck, M., et al., The pairwise phase consistency: A bias-free measure of rhythmic neuronal synchronization, NeuroImage (2010), doi:10.1016/j.neuroimage.2010.01.073

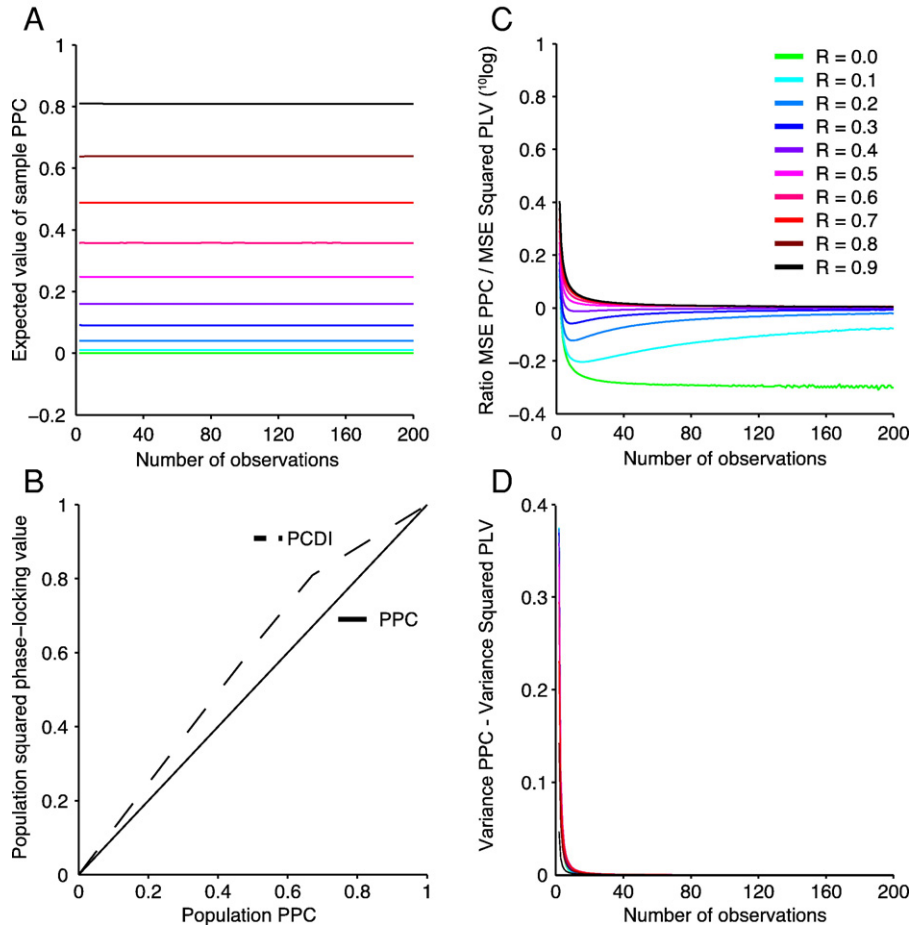

Fig. 3. Comparison of PPC (pairwise phase consistency) to phase-locking value (PLV). (A) PPC estimate versus sample size. PPC estimate does not have any bias. Samples were drawn from von Mises distribution. Corresponding population PLV is given in legends of (C) Comparison of PPC (pairwise phase consistency) to phase-locking value (PLV). (A) PPC estimate versus sample size. PPC estimate does not have any bias. Samples were drawn from von Mises distribution. Corresponding population PLV is given in legends of (C). Lowest green line corresponds to uniform distribution. (B) Relationship squared PLV, PPC and PCDI. The population value of the PPC is identical to the population value of the squared PLV. For PLV values smaller than 0.9, a near linear relationship is observed between the PCDI and the squared PLV (regression weight for PLV values smaller than 0.9 is 1.21). (C) Comparison of MSE (mean squared error) for PLV and PPC. *Y*-axis: ratio of MSE for PPC to MSE for PLV (log transformed). *X*-axis: number of observations. Value of zero indicates that MSE is the same for both statistics. Values lower than zero indicate that MSE is smaller for PPC than for squared PLV. For low values of the PLV (0–0.3), we obtain a smaller MSE for the PPC. For higher values of the PLV, the MSE of PPC is only slightly greater than the MSE of the squared PLV. Color coding indicates different PLV (resultant length) values. (D) Comparison of variance for squared PLV with variance of PPC. A value of zero indicates equal variance. Variance of squared PLV and PPC are comparable for sample sizes larger than 10. (For interpretation of the references to colour in this figure legend, the reader is referred to the web version of this article.)

The PPC has several advantages to the coherence and PLV in several respects. A main advantage is that the PPC's sample estimate has no bias. Experimentally, this is especially an advantage when the sample consists of spike phases from sparsely firing neurons, or when the number of behavioral trials depends on the response of the behavioral subject and not on the experimenter. The unbiasedness gives several advantages. First, in neuroscience we often average results across subjects or neurons, because individual measurements are often relatively noisy. When there is a systematic bias across subjects or neurons, then this bias will appear in the group average as well. However, when the error of the sample estimates (relative to the population statistic) is only determined by the variance of the sample estimates, then we can squeeze this variance out of our group average, since it is expected to be largely independent across subjects or neurons. Unbiasedness ensures that our data will not have a systematic tendency for false positives. At the same time, unbiasedness increases the sensitivity of our statistical comparisons. A difference in sample size, which causes the PLV to go in the opposite direction of a hypothesized effect, will not affect the PPC. Second, unbiasedness facilitates the comparison of outcomes across different experiments. Such a comparison is currently complicated because of the sample-size bias. Depending on the behavioral task and recording area, large differences in the number of recorded spikes per neuron or behavioral trials can exist. The comparison of the strength of rhythmic synchronization across areas and stimulus and behavioral condition takes place mostly across experiments, and the sample size might be very different between experiments. Thus, we expect that the use of the PPC can give rise to interesting meta-analyses across experiments. Third, some research questions are explicitly concerned with the relationship between firing rates and rhythmic synchronization: a bias-free measure of rhythmic synchronization is very important in these cases. Another main advantage of the PPC is that the PPC has a smaller MSE (mean squared error) than the PLV. This means that the reduction in bias does not come at the expense of an even larger variance. Despite these advantages of the PPC, it should be emphasized that the PLV (and the coherence) remain important descriptive measures of the data. Although the PPC provides an unbiased estimate of the population value of the squared PLV, it does not for the PLV itself. The current paper did not investigate under what conditions the PLV can be reliably estimated from the square root of the PPC. Since the sample estimator of the PPC can attain negative values, this is at least impossible for combinations of lower values of the (population) PLV and PPC and small sample sizes.

As already argued in the methods, the PPC also compares favorably to the FSPLV. First, the FSPLV is not an unbiased measure, in the sense that different types of circular distributions (e.g., unimodal vs.

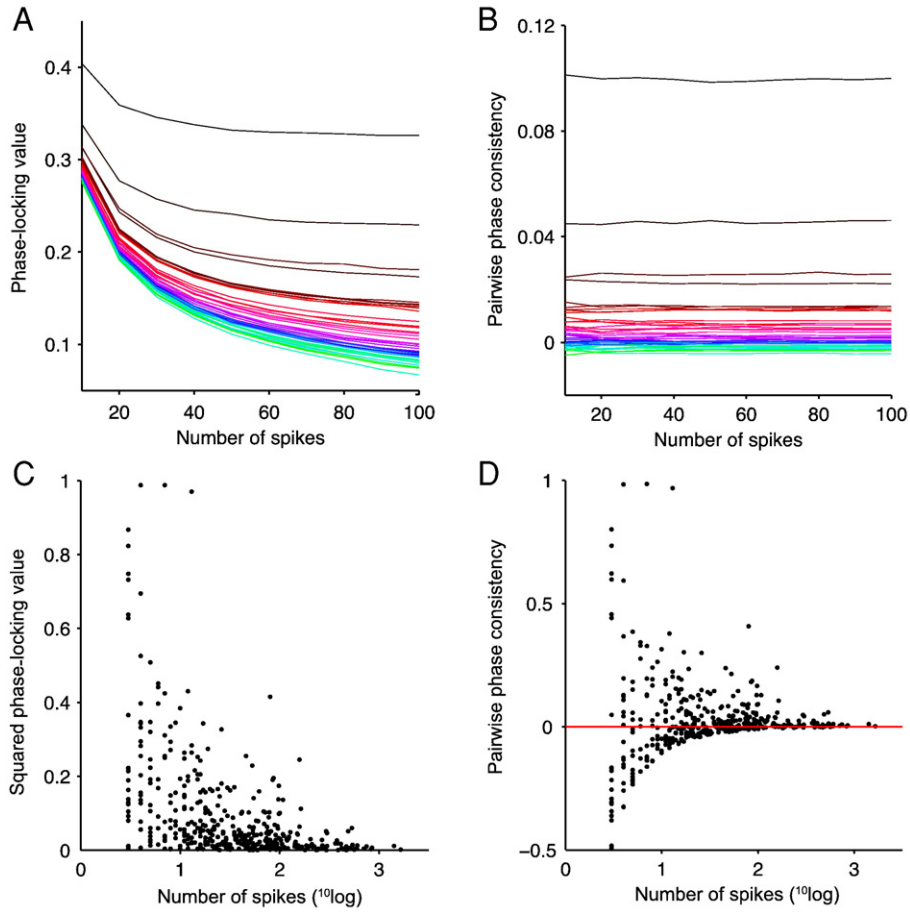

Fig. 4. Application of pairwise phase consistency (PPC) to neuronal data. (A) Bias of PLV (phase-locking value) as a function of spike count for individual cells. Theta-band spike–LFP synchronization was investigated while rats anticipated reward at a fluid well. For neurons with more than 200 spikes during reward anticipation period, we drew samples of different sizes from the distribution of all recorded spike theta (6 Hz) phases. 10 PLV showed a strong bias as a function of sample size. Every line corresponds to a single unit. Color scale indicates different levels of phase consistency. (B) Bias of PPC as a function of number of spikes for individual cells. Same conventions as in (A), expect that here the PPC is plotted. PPC showed no bias as a function of sample size. (C) Distribution of squared PLVs across neuronal population. Each dot represents a neuron. All recorded spikes were used to calculate the squared PLV. Neurons with few recorded spikes demonstrated higher squared PLV. (D) Distribution of PPC across neuronal population. Same conventions as in (C), except that here the PPC is plotted. The strong bias of the PLV (C) disappeared for the PPC. Application of pairwise phase consistency (PPC) to neuronal data. (A) Bias of PLV (phase-locking value) as a function of spike count for individual cells. Theta-band spike–LFP synchronization was investigated while rats anticipated reward at a fluid well. For neurons with more than 200 spikes during reward anticipation period, we drew samples of different sizes from the distribution of all recorded spike theta (6 Hz) phases. 10 PLV showed a strong bias as a function of sample size. Every line corresponds to a single unit. Color scale indicates different levels of phase consistency. (B) Bias of PPC as a function of number of spikes for individual cells. Same conventions as in (A), expect that here the PPC is plotted. PPC showed no bias as a function of sample size. (C) Distribution of squared PLVs across neuronal population. Each dot represents a neuron. All recorded spikes were used to calculate the squared PLV. Neurons with few recorded spikes demonstrated higher squared PLV. (D) Distribution of PPC across neuronal population. Same conventions as in (C), except that here the PPC is plotted. The strong bias of the PLV (C) disappeared for the PPC. (For interpretation of the references to colour in this figure legend, the reader is referred to the web version of this article.)

bimodal) can have a different dependence of the sample FSPLV on sample size. Second, to use the FSPLV, an arbitrary value has to be chosen (the fixed number of observations we use per sample). Different choices of this value might result in different conclusions. Moreover, if we choose different parameter values of F across different experiments, it will be hard to compare the degree of phase consistency across experiments, because we are essentially using a different population statistic in every experiment. Finally, some subjects or neurons might not have enough trials or spikes to compute the FSPLV, so that results might not generalize to the whole population. For the PPC, all subjects and neurons can contribute to the group average. Third, the PPC uses all available data, whereas for the FSPLV, it is typically not practical to use all available data in the same way, because computing all possible bootstraps is computationally often not feasible. That means that some observations might appear more often in the bootstraps than other samples and that some combinations of observations are not taken into account. This will lead to a higher variance of our sample estimates and also a variance of the outcomes from run to run. The PPC leads to exactly the same outcome every time we compute it.

The main disadvantage of the PPC is that it is computationally inefficient (order N larger) in comparison to the PLV and the coherence. However, N^2 computations are still practically feasible, which is demonstrated by the fact that we could easily compute the PPC across 525 neurons. Another potential disadvantage is that negative values are possible when using the normalized version of the PPC (whose expected value runs from 0 to 1). This is a consequence of the unbiasedness of the PPC. In general, if a statistic is bounded from below by zero, then its expected value can only be zero then the variance is zero. On the contrary, the PLV estimate has the highest variance when its population value is zero. Percentages of change can only be computed when all values are larger than zero, so we might not be able to compute percentages in all cases. On the other hand, the percentage of change that can be obtained (when the values are positive) will not be influenced any more by the sample size (thus it will be larger). For the PLV and coherence, we will typically obtain smaller effect sizes, because small sample sizes effectively decrease the dynamic range of the statistic. Often, it is not even clear what the dynamic range of reported PLV or coherence values is. The PPC has the advantage that it has the same dynamic range, regardless of the

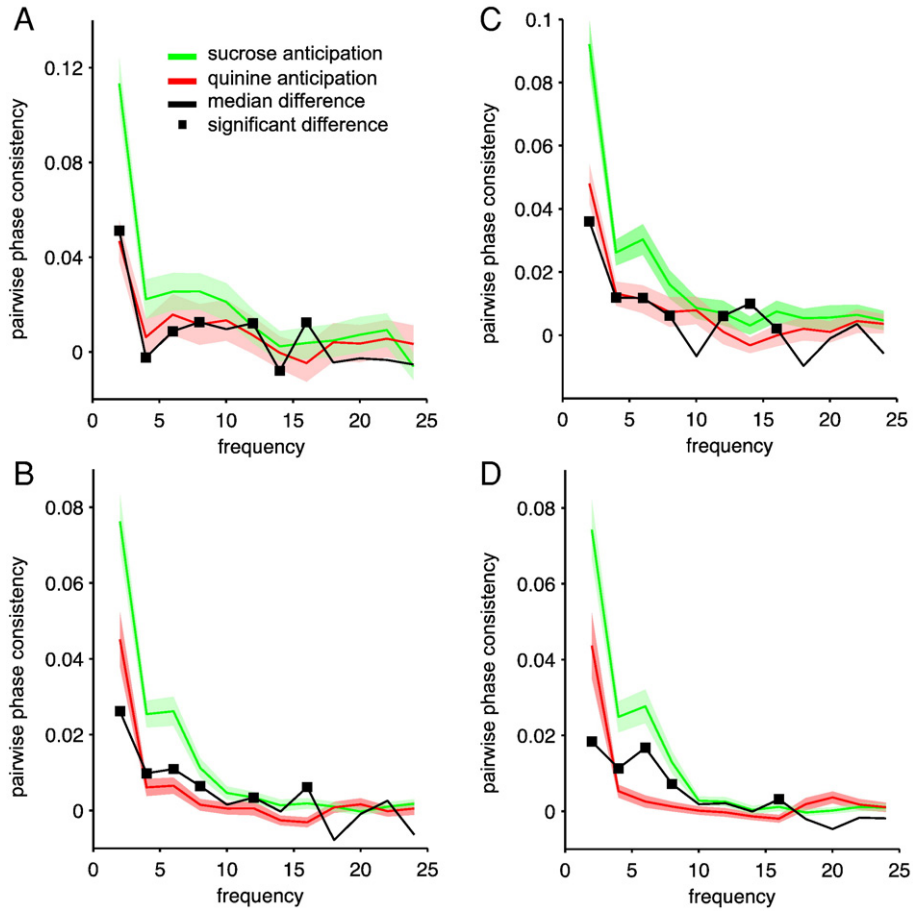

Fig. 5. Application of pairwise phase consistency (PPC) to neuronal data. (A) We compared rhythmic spike–LFP synchronization while rats anticipated either sucrose (correct Go response) or quinine (incorrect Go response). Green solid line: mean PPC across all recorded neurons for sucrose anticipation. Red solid line: mean PPC across all recorded neurons for quinine anticipation. Black solid line: median difference of PPC between sucrose and quinine anticipation. Black squares: significant frequencies (*P* Application of pairwise phase consistency (PPC) to neuronal data. (A) We compared rhythmic spike–LFP synchronization while rats anticipated either sucrose (correct Go response) or quinine (incorrect Go response). Green solid line: mean PPC across all recorded neurons for sucrose anticipation. Red solid line: mean PPC across all recorded neurons for quinine anticipation. Black solid line: median difference of PPC between sucrose and quinine anticipation. Black squares: significant frequencies ($P<0.05$, Rank-Wilcoxon). Shades: standard error of the mean. All neurons ($N=525$) were included to compute averages. Even when including all cells, including those with high variance of the PPC estimate, the difference between the sucrose and quinine anticipation condition is already apparent for a broad range of low frequencies. (B) Same as in (A), but now including all neurons with more than 10 recorded spikes. Note how the difference between quinine and sucrose anticipation becomes more visible because we removed units with very high variance (because of low number of recorded spikes). For quinine, a complete absence of rhythmic synchronization at 15 Hz is observed. (C) Same as in (A) and (B), but now for neurons with more than 30 recorded spikes. (D) Same as in (A) to (C), but now for neurons with more than 50 recorded spikes. (For interpretation of the references to colour in this figure legend, the reader is referred to the web version of this article.)

number of samples we take. As a rather philosophical remark, we would like to point out that a percentage increase in the degree of phase consistency (e.g., a 100% change from 0.05 to 0.1) can as well be interpreted as a much smaller decrease in the amount of randomness of our spikes if we had let our scale of randomness run from 0 to 1 instead of 1 to 0 (e.g., a 5% decrease from 0.95 to 0.9).

Finally, we demonstrated the use of the PPC in neuronal data. Spiking activity from orbitofrontal neurons was recorded from well isolated sparsely firing neurons, while the rat engaged in a two-odour discrimination task. We demonstrated that the PLV was influenced by the firing rate, while the PPC was not. Furthermore, we demonstrated the use of the PPC by analyzing group differences in spike–LFP rhythmic synchronization during different task conditions. We showed that for a large range of low frequencies, rhythmic synchronization was selectively enhanced during anticipation of sucrose delivery versus anticipation of quinine delivery.

To conclude, we provide a measure of rhythmic synchronization, which is easily computed, has an unbiased and consistent estimator, an intuitive interpretation and is straightforwardly related to existing measures of rhythmic synchronization. We expect that, for many experimental questions, our method will provide increased sensitivity for true positives and a decreased sensitivity for false negatives in comparison to existing methods. The pairwise phase consistency has great applicability when we want to measure rhythmic synchronization for both EEG–EEG, MEG–MEG, spike–LFP, and spike–spike pairs but might very well be applicable in the biomedical sciences in general and other sciences (e.g., physics or geosciences) in which circular statistics play an important role.

Acknowledgments

We thank Prof. A.J. Vinck, Dr. Jan Lankelma, Dr. Franscesco Battaglia and Dr. Conrado Bosman for helpful comments. Furthermore, we would like to acknowledge the developers of Fieldtrip (fieldtrip.fcdonders.nl), in particular Dr. Robert Oostenveld; Peter Lipa (University of Arizona, Tucson AZ) for the use of BubbleClust; and A. David Redish (University of Minnesota, Minneapolis MN) for the use of MClust.

References

Best, D., Fisher, N., 1979. Efficient simulation of the von mises distribution. J. R. Stat. Soc. Ser. C (Appl. Stat).

ARTICLE IN PRESS

Buschman, T.J., Miller, E.K., 2009. Serial, covert shifts of attention during visual search are reflected by the frontal eye fields and correlated with population oscillations. Neuron 63, 386–396.
Buzsáki, G., Draguhn, A., 2004. Neuronal oscillations in cortical networks. Science 304, 1926–1929.
Fisher, N., 1993. Statistical analysis of circular data. Cambridge University Press.
Fries, P., 2005. A mechanism for cognitive dynamics: neuronal communication through neuronal coherence. Trends Cogn. Sci. 9, 474–480.
Fries, P., 2009. Neuronal gamma-band synchronization as a fundamental process in cortical computation. Annu. Rev. Neurosci. 32, 209–224.
Fries, P., Nikoli, D., Singer, W., 2007. The gamma cycle. Trends Neurosci. 30, 309–316.
Fries, P., Womelsdorf, T., Oostenveld, R., Desimone, R., 2008. The effects of visual stimulation and selective visual attention on rhythmic neuronal synchronization in macaque area V4. J. Neurosci. 28, 4823–4835.
Gray, C.M., Koenig, P., Engel, A.K., Singer, W., 1989. Oscillatory responses in cat visual cortex exhibit inter-columnar synchronization which reflects global stimulus properties. Nature 338, 334–337.
Gregoriou, G.G., Gotts, S.J., Zhou, H., Desimone, R., 2009. High-frequency, long-range coupling between prefrontal and visual cortex during attention. Science 324, 1207–1210.
Hopfield, J.J., 1995. Pattern recognition computation using action potential timing for stimulus representation. Nature 376, 33–36.
Jarvis, M.R., Mitra, P.P., 2001. Sampling properties of the spectrum and coherency of sequences of action potentials. Neural Comput. 13, 717–749.
Lachaux, J.P., Rodriguez, E., Martinerie, J., Varela, F.J., 1999. Measuring phase synchrony in brain signals. Hum. Brain Mapp. 8, 194–208.
Lansink, C.S., Goltstein, P.M., Lankelma, J.V., Joosten, R.N., McNaughton, B.L., Pennartz, C. M., Jun. 2008. Preferential reactivation of motivationally relevant information in the ventral striatum. J. Neurosci. 28, 6372–6382.
Mitra, P.P., Pesaran, B., Feb. 1999. Analysis of dynamic brain imaging data. Biophys. J. 76, 691–708.
O'Keefe, J., Recce, M.L., 1993. Phase relationship between hippocampal place units and the EEG theta rhythm. Hippocampus 3, 317–330.
Pesaran, B., Pezaris, J.S., Sahani, M., Mitra, P.P., Andersen, R.A., 2002. Temporal structure in neuronal activity during working memory in macaque parietal cortex. Nat. Neurosci. 5, 805–811.
Pesaran, B., Nelson, M.J., Andersen, R.A., 2008. Free choice activates a decision circuit between frontal and parietal cortex. Nature 453, 406–409.
Quyen, M.L.V., Foucher, J., Lachaux, J., Rodriguez, E., Lutz, A., Martinerie, J., Varela, F.J., 2001. Comparison of hilbert transform and wavelet methods for the analysis of neuronal synchrony. J. Neurosci. Methods 111, 83–98.
Sejnowski, T.J., Paulsen, O., 2006. Network oscillations: emerging computational principles. J. Neurosci. 26, 1673–1676.
Siapas, A.G., Lubenov, E.V., Wilson, M.A., 2005. Prefrontal phase locking to hippocampal theta oscillations. Neuron 46, 141–151.
Singer, W., Gray, C.M., 1995. Visual feature integration and the temporal correlation hypothesis. Annu. Rev. Neurosci. 18, 555–586.
Sirota, A., Montgomery, S., Fujisawa, S., Isomura, Y., Zugaro, M., Buzsa 'ki, G., 2008. Entrainment of neocortical neurons and gamma oscillations by the hippocampal theta rhythm. Neuron 60, 683–697.
Varela, F., Lachaux, J.P., Rodriguez, E., Martinerie, J., 2001. The brainweb: phase synchronization and large-scale integration. Nat. Rev. Neurosci. 2, 229–239.
Vinck, M., Lima, B., Womelsdorf, T., Oostenveld, R., Singer, W., Neuen-schwander, S., Fries, P., 2009. Gamma-phase shifting in awake monkey visual cortex. J. Neurosci.
Womelsdorf, T., Schoffelen, J.M., Oostenveld, R., Singer, W., Desimone, R., Engel, A.K., Fries, P., 2007. Modulation of neuronal interactions through neuronal synchronization. Science 316, 1609–1612.
Womelsdorf, T., Lima, B., Vinck, M., Oostenveld, R., Bosman, C., E.A., B., Desimone, R., Singer, W., Neuenschwander, S., Fries, P., 2008. Putative excitatory and inhibitory neurons synchronize at different phases of the gamma cycle in visual areas V1 and V4 of awake monkeys. Society of Neuroscience Abstracts, 38th Annual Meeting, Washington D.C., USA.

Please cite this article as: Vinck, M., et al., The pairwise phase consistency: A bias-free measure of rhythmic neuronal synchronization, NeuroImage (2010), doi:10.1016/j.neuroimage.2010.01.073